ISTANBUL TECHNICAL UNIVERSITY ★ GRADUATE SCHOOL OF SCIENCE ENGINEERING AND TECHNOLOGY

EXPERIMENTAL INVESTIGATION OF SWIRL STABILIZED FLAMES

M.Sc. THESIS

Bertan KAYNAROĞLU

Department of Defence Technologies

Defense Technologies Programme

05/2014

ISTANBUL TECHNICAL UNIVERSITY ★ GRADUATE SCHOOL OF SCIENCE ENGINEERING AND TECHNOLOGY

EXPERIMENTAL INVESTIGATION OF SWIRL STABILIZED FLAMES

M.Sc. THESIS

Bertan KAYNAROĞLU
(514111002)

Department of Aeronautical Engineering

Defense Tecnologies Programme

Thesis Advisor: Assoc. Prof. Onur TUNÇER

05/2014

İSTANBUL TEKNİK ÜNİVERSİTESİ ★ FEN BİLİMLERİ ENSTİTÜSÜ

GİRDAP VANESİ İLE STABİLİZE EDİLMİŞ ALEVLERİN DENEYSEL İNCELENMESİ

YÜKSEK LİSANS TEZİ

Bertan KAYNAROĞLU
(514111002)

Savunma Teknolojileri Departmanı

Savunma Teknolojileri Programı

Tez Danışmanı:Doç. Dr. Onur TUNÇER

05/2014

Bertan Kaynaroğlu, a **M.Sc.** student of ITU **Graduate School of Science Engineering and Technology** student ID **514111002**, successfully defended the **thesis** entitled "**EXPERIMENTAL INVESTIGATION OF SWIRL STABILIZED FLAMES**", which he prepared after fulfilling the requirements specified in the associated legislations, before the jury whose signatures are below.

Thesis Advisor :	**Assoc. Prof. Dr. Onur TUNÇER** İstanbul Technical University	.....
Jury Members :	**Prof. Dr. N. L. Okşan ÇETİNER - YILDIRIM** İstanbul Technical University	.....
	Prof. Dr. Cem SORUŞBAY İstanbul Technical University	.....

Date of Submission : 05 May 2014
Date of Defense : 29 May 2014

To my family,

FOREWORD

Foremost, I would like to express my sincere gratitude to my advisor Assoc. Prof. Dr. Onur TUNÇER for his supports and encouragement through my studies. It has been an honour to work with him. I also thank him for his patience to my English writing skills during the writen papers and also for this thesis.
Then, I would like to thank Assoc. Prof. Dr. N. L. Okşan Çetiner YILDIRIM for her constructive comments and suggestions. I also thank to Murat SARITAŞ, for his feedbacks on my experiments and Serdar SEÇKİN deserves my lots of appreciation for his misterious touches on my MATLAB code. I thank to Onur SON, Mahmut Can KARAKAYA, Selin KAHRAMAN and Gürkan SARIKAYA for the efforts during my experiments and for their precious friendships.
I gratefully acknowledge the financial support received from the Turkish Scientific and Technical Research Council (TÜBİTAK) under contract number 109M426.
Last but not least, I gratefully thank to Gizem DEDEOĞLU and my family for their endless support. Also I would like to thank Trisonik Laboratory collogues for a friendly environment.

June 2014 Bertan KAYNAROĞLU

TABLE OF CONTENTS

Page

ABBREVIATIONS

PIV **:** Particle Image Velocimetry
ISL **:** Inner Shear Layer
OSL **:** Outer Shear Layer
VBB **:** Vortex Breakdown Bubble
IRZ **:** Inner Recirculation Zone
ORZ **:** Outer Recirculation Zone
FFT **:** Fast Fourier Transform

LIST OF FIGURES

Page

EXPERIMENTAL INVESTIGATION OF SWIRL STABILIZED FLAMES

SUMMARY

In this thesis, under atmospheric working conditions a swirl stabilized pre-mixed burner was constructed in order to reveal flame characteristics and the interaction between flame front and turbulent flow properties. Swirl number of the combustor was 0.74 and equivalence ratio was selected as 0.7. Through this thesis flow structure of cold flow and reacting flow was presented primarly for an early diagnostic. Then much of the effort was concentrate on image processing to reveal the flame fronts from PIV images.

Swirl burner was designed to has eight blades with 45˚ with respect to oncoming flow. Two different type of seeder particles were used for different purposes which can be named for inspection for the whole area flow and to acquire flame front position with its details.

For this purpose, cold flow properties were revealed by using Particle Image Velocimetry (PIV) technique. At this stage, interrogation window size set to 64 x 64 pixels and overlapping with 50% in order to observe overall flow properties. TiO_2 particals and oil dropelts were used to seed to flow. By the nature of the flow property, big particals under the centripetal forces tend to move outside of the exit of the burner. TiO_2 particles pertain this phenomena due to agglomeration even if the high humidity inside the seeder drum was removed by simple heaters. For the PIV calculations, average correlation method was used instead of cross correlation method which is widely-used. Average correlation method was chosen since it is a convenient method when the seed particle density changes dramatically within the flow field.

In reacting flow case a similar flow structure has been observed. Two recirculation regions which can be named as inner and outer recirculation regions. Inside the inner recirculation region adverse pressure gradient occur due to sudden expansion of the oncoming flow creating a reserve flow over the center body flame holder. Beside of that a weak recirculation region occurs at the edge of the dump plane due to interaction of the swirling flow with the stagnant air out of the investigated region. However, at the burnt side particle density decreases due to thermal expansion in this region which increase the capability of edge detection algorithm kindly.

Flame fronts were revealed by using Canny edge detection algorithm. Flame front characteristics as turbulent burning velocity and wrinkling factors figured out by using a MATLAB algorithm.

GİRDAP VANESİ İLE STABİLİZE EDİLMİŞ ALEVLERİN DENEYSEL İNCELENMESİ

ÖZET

Bu tez kapsamında, atmosferik şartlar altında açık, ön-karışımlı bir yakıcının alev karakteristiği ve türbülanslı akış ile etkileşimi incelenmiştir. Akış yapısı ortaya konularak alevin kararlı bir şekilde kalmasının fiziksel incelemesi yapılmıştır.
Deney düzeneği olarak sekiz paleli ve gelen akışa 45 ° ile yerleştirilmiş konvansiyonel bir girdap vanesi ile ortasında alev tutucu bir çubuk bulunan girdap üreteci kullanılmıştır. Çubuğun bittiği konumda akış genişleme düzlemine ulaşmaktadır.
Bu amaçla ilk başta soğuk akışın özellikleri Parçacıkla Hız Tayini (PIV) yöntemi ile incelenmiş olup akış yapısı ortaya çıkarılmıştır. Bu aşama da sorgulama penceresi akış yapısının genel özelliklerinin elde edilmesi amacı ile 64 x 64 piksel ve % 50 üst üste bindirme ile elde edilmiştir. Soğuk akış incelemelerinde parçacık olarak hem TiO_2 hem lazkin nozülünde hava parçalamasına uğramış yağ partükülleri kullanılmıştır. Akışın özelliği olarak merkezcil kuvvetler etkisi altında büyük parçalı ve her ne kadar ön kurutmaya tabi tutulsa da sıkıştırılmış havadan gelen nem yüzünden topaklanan TiO_2 parçacıkları çıkış kesitinin dış kısımlarına doğru yönlenmiştir. Bu yöntemle PIV ölçümlerinde ki sinyal gürültü oranını düşürdüğünden dolayı zaman zaman hatalı vektörler vermektedir. Bu yüzden, yağ damlacıkları deneyler de öncelikli olarak tercih sebebi olmuştur. PIV ölçümlerinden hız vektörleri bulunurken çok bilindik bir yöntem olan çapraz korelasyon yerine ortalama korelasyon alınmıştır. Ortalama korelasyon yöntemi, belirlenen sorgulama penceresinin her bir görüntüde ki toplamını alıp sonrasında ortalamasını alır. Bu ortalamayı ikinci resimde ki ortalama ile korelasyona uğratarak bu sorgulama penceresinden bir vektör elde eder. Sonrasında bu işlem her bir sorgulama penceresine uygulanarak hız vektör alanı elde edilmiş olur. Bu yöntem çapraz korelasyonun aksine hem daha hızlı hemde daha güvenilir sonuçlar vermiştir. Bu nedenle hız vektörleri üzerinde hiç bir yumuşatma olmadan, gerçek hız vektörleri elde edilmiştir.
Akışın genel özelliği olarak, iki farklı yeniden dolaşım bölgesi gözlenmiş, bunlardan biri içte olup iç yeniden dolaşım bölgesi olarak adlandırılmış. Gelen akış yakıcıdan çıkarken genişlemeye uğrayarak alev tutucu çubuğun üzerinde ters bir basınç gradyeni ile güçlü bir yeniden dolaşım bölgesi oluşturmaktadır. İkinci bir zayıf yeniden dolaşım bölgesi ise yakıcının dış taraflarında durgun hava ile etkileşim sonucu oluşmaktadır.
Tepkimeli akış incelemelerinde eşdeğerlik oranı TiO_2 parçağı ile yapılan deneylerde 0.74, yağ parçacıkları ile yapılan deneylerde 0.7 olarak sönme bölgesinden hemen üstünde bir değerde yapılmıştır. Bu deneylerde soğuk akış ile benzer bir akış yapısı gözlenmiştir. Tepkimeli akış görüntülemesi akışın bütün özelliklerini incelemek anlamında sorgulama penceresi soğuk akışla aynı olacak şekilde seçilmiştir. Akış karakteristiği için TiO_2 partikülleri kullanılmış ve yanmış gazların soğuk akışta

olduğu gibi iç bölgede yeniden dolaşım bölgesini oluşturuduğu görülmüştür. İç sınır tabakaya bağlı kalarak gelişen bu durum sonucunda iç yeniden dolaşım bölgesinde "V" şeklinde bir alev oluşturduğu gözlenmiştir. Bu yeniden dolaşım bölgesi akış özellikleri göz önüne alındığında bu bölgede yanma sırasında oluşan ara geçiş ürünleri olan radikalleri hapsetmiş ve bu sayede yanma sonucu oluşan ürünlere geçişi kolaylaştırarak alevin fakir olarak yanmasına katkı sağlamıştır. Ayrıca girdap vanesi sayesinde akışın girdap şeklinde olması 3-boyutluluk göz önüne alındığında taze hava-yakıt karışımı alev cephesinin ısısına daha fazla maruz kalmış ve gelen akışın sıcaklığı yükseltilmiştir. Bu kısımda unutulmamalıdır ki, ortalama korelasyon alevin salınma özelliğinden dolayı doğru sonuçlar vermeyecektir. Bu yüzden bu kısımda ki hız vektörleri çapraz korelasyon yöntemi ile elde edilmiştir.

TiO_2 ile yapılan deneylerde alevin yanmış gazları ısıtmasından dolayı bu bölgede ısıl genişleme olmasından ötürü parçacık yoğunluğu soğuk akışa göre ciddi bir şekilde azalmıştır. Buna rağmen alev cephesinin alanı bu gradyen değişiminden dolayı kolayca bulunacak hale gelmiştir. PIV ile kaydedilen Mie saçılım görüntülerinden bu sonuç çıplak gözle dahi görülebilmektedir.

Ortaya konulan akış yapısından sonra alev cephesinin özellikleri incelenmiştir. Alev cephesinin özellikleri hem yukarı da bahsedilen TiO_2 parçacıkları ile gözlenmiş hemde yağ partikülleri ile çalışma daha ileriye taşınmıştır. Alev cephesinin ortalama özellikleri, TiO_2 ile yapılan deneylerde ortaya konmuştur. Bunun için görüntüler üst üste toplanmış sonrasında ise keskin gradyen bulunmaya çalışılmıştır. Yağ partikülleri ile yapılan deneylerde ise, yağ partikülleri alev cephesinden ürünler kısmına doğru geçerken yanmakta ve gözden kaybolmaktadır. Bu sayede her bir görüntüde keskin bir alev cephesi çıplak gözle dahi gözükmektedir. Alev cepheleri MATLAB'da yazılan algoritma ile bulunmaya çalışılmıştır. Bu algoritma ise şu şekilde ilerlemektedir: ilk başta PIV görüntülerine Gauss filtesi vb. filtreler uygulanarak her hangi bir yanlış girinti çıkıntı alev cephesinde yumuşatılmıştır. Bu noktada alev sınırının detaylı özelliğini tutmadan sadece genel olarak filtreleme yapılmıştır. Medyan ve Weiner filtreleri kenar özelliklerini koruduğundan dolayı girintili ve çıkıntılı alev yapısı özelliği korunmaya devam edilmektedir bu da haylice hataya yol açmaktadır. Buna ek olarak filtre sonucu elde edilen hatanın beş piksel mertebesinde olmasından dolayı filtrelereme konusundan herhangi bir hataya yol açılmamıştır. Filtreler sırasında elde edilen görüntünün parlaklık histogramı çizdirilmiş ve buna göre histogramı genişletilmiş ve eş dağılımlı olması göz önüne alınmıştır. Tam bu anda görüntü daha da işlenmeden önce soğuk reaktantlarların olduğu bölge beyaz, ürünlerin olduğu bölge siyah olacak şekilde ikili matrise dönüştürülmüştür. Fakat bu nokta da alev cephesinin belirlenmesi için çok fazla girintili çıkıntılı olduğuna karar verilmiş ve görüntüyü pürüzsüzleştirme işlemine devam edilmiştir. Bir adım daha pürüzsüzleştirme uygulamak açısından, görüntü 5 piksel çapında disk şeklinde bir matris ile korele edilmiştir. Bu adımla birlikte görüntüler kenar sınırları bulunmak için yeterli düzgünlüğe ulaşmıştır. Bu adımdan sonra görüntü yanmamış reaktantlar bir, yanmış ürünler sıfır olacak şekilde ikili bir matris ile ifade edilmiştir. Kenar sınır algoritması olarak Canny'nin geliştirdiği metod kullanılmış ve başarılı olunmuştur. Eşik değeri düzgün bir biçimde arttırılarak üst üste iki kere Canny sınır belirleme algoritması kullanılmıştır. Sonrasında ise elde edilen görüntü alev cephesinin olmasının beklendiği alan maskelenerek sadece bu bölge ile ilgilenilmiştir. Bazı kenarların kopuk olduğu görüldüğünden Canny'nin alev cephesini tek piksel ile sembolize eden algoritmasına, bu cephenin kalınlaştırılıp tekrar inceltilmesi medotu eklenerek alev cephesinin her koşulda sürekli olarak temsil edilmesi sağlanmıştır.

Elde edilen alev cepheleri, ortalama alev cephesi alanı ile anlık alev cepheleri alanları bulmak ve buradan türbülanslı yanma hızına geçmek için görüntüler işlenmeye devam edilmiştir. Damköhler'in türbülanslı alev tanımı ışığı altında ve alev cephesi alanları ile laminer alev ilerleme hızını bilerek türbülanslı alev hızları elde edilmiştir. Her bir görüntü sonucu elde edilen alev cephelerinin alanları bir resimde toplanarak alev fırçası kalınlığı (flame brush thickness) elde edilmiştir. Bu elde edilen bilgi, Hesaplamalı Akışkanlar Dinamiği (HAD) çözümlemeleri için oldukça önemlidir. Alev fırçası kalınlığı, çözüm yapılacak alanda alev cephesinin konumunun ulaşabileceği en uç noktaları temsil eder. Bu değer, akış alanının ağ yapısı oluşturulurken dikkate alındığında en küçük yapıdaki türbülans özelliklerini bulma konusunda hayli önem teşkil eder ve hem türbülans hem de alevin özelliklerini bulma konusundan HAD çözümlemeleri için doğru sonuçlar verir. Yapılan bu çalışma ile artan ve kıvrımlaşan alev alanı ile türbülanslı alev ilerleme hızının arttığı gözlenmiştir. Alev cephelerinin bulunduğu flame brush bölgesinde bir nokta seçilerek bu noktadaki dik hız bileşeni ile alev alanlarının faz diagrami çizdirilmiş ve herhangi bir korelasyon gözlenmemiştir. Aynı şekilde düşey düzlemde alev cephelerinin salınımına dair baskın bir frekansta gözlenmemiştir. Fakat unutulmamalıdır ki, girdaplı akış yatay düzlemde ki hareketi frekans ve salınım hareketine sahip olabilir.

1. INTRODUCTION

Due to increased demand on energy and transportation systems use of fuel come into prominence. Even if this huge demand on energy tried to be provided with renewables, triple increase in renewable energy over the next 25 years, the world is likely still to depend on fossil fuels for at least 50 percent of its energy needs [1]. At the same time, decreasing and awaiting of possible extinction of fossil fuels in near future, it must be used efficiently.

Increased environmental problems owing to residual CO_2 within atmosphere, along with efficiently used fuels should be spend with sustainable way. Therefore, power and energy producer combustion systems have been enhanced also with the help of governmental obligations. However, these improvements do not satisfy the NO_x emission requirements. New combustor systems were introduced to meet these necessities. Popular research area of the recent years is swirl stabilized premixed combustors. Present thesis focuses on this phenomenon.

One to above reasons, lean premixed combustion came forward as a much discussed topic in recent years. However, interaction with turbulence and chemistry is not well defined and it is believed that it is almost impossible to define the interaction in analytical methods. Thus more attention is focused on the outcomes of experiments. This thesis firstly deals with aerodynamic effects on flame stabilization then flame characteristics of premixed swirling flames are handled.

As an experimental technique, Particle Image Velocimetry (PIV) is used to reveal the flow characteristics of the burner. Statistical analysis on turbulent flames presented due to aptitude of the simultaneous PIV technique. Furthermore, turbulent combustion parameters were tried to be revealed from the images obtained from PIV, such as flame front positions, shape and fluctuation parameters.

Next chapter provides brief information about the literature and theoretical aspects of the topic under investigation. Chapter 2 discusses the details about experimental setup and measurement methodology. Results and comments on the findings of

experiments are presented in Chapter 3. Finally, Chapter 4 provides a comprehensive conclusion and recommendation for further studies.

1.1 Purpose of Thesis

The purpose of this thesis is to give a brief understanding on turbulence and chemistry interactions on a premixed swirl stabilized burner with different experimental approaches. To achieve these goals fundamental properties and characteristics should be well defined which can be referred as flame front position with respect to oncoming flow, its fluctuation, flame shape and turbulent flame speed. Complete understanding of an open flame configuration may lead to practical application on stabilized and cleaner combustion for industry and aviation. As side inference, experimental results on flow and flame characteristics presented for validations of further numerical study.

1.2 Literature Review

In this chapter theory of lean turbulent premixed combustion is discussed. While beginning parts introduce the combustion and turbulent flow properties, last part gives brief discussions on flame characteristics relavent to image processing.

1.2.1 Lean premixed combustion

Before premixed combustion became popular, a great number of burners were operated with diffusion flames. This kind of combustion process is widely used after pressure swirl-spray atomizers are created [2]. Due to poor mixing characteristics of this type of burners, high rate of soot formation and low efficiency problems were revealed in the literature [3-5]. However, these properties have positive influence on combustion stability and flame stays within extinction limits somehow. Since then, governmental regulations based on emission requirements, especially for aviation, have an increased trend in recent decade which cause modern gas turbine combustors work under lean conditions. Thereby, achievement of lowering flame temperatures cause to reduced NO_x emissions. On the other hand, premixed combustion has also its drawbacks as if the mixture get leaner, flame could reach extinction.

1.2.1.1 Lean Blowout

Lean blowout limits of a combustor must be well defined in order not to cause flame extinction. Owing to safety hazards and sophisticated shutdown and restart procedures, blowout is a highly undesirable situation. Lean blowout is believed to be extended depending on different parameters as increasing swirl number [7] and air inlet temperature[2], addition of hydrogen [8,9,10].

1.2.2 Turbulent flames

The first explanation of turbulent flame propagation is due to Damköhler [11]. Damköhler defines two distinct regimes which are called small and large scale turbulence. For small scale turbulence, turbulent eddies modify the transport mechanism within the reaction zone which is named as preheat zone. For large-scale turbulence on the other hand, turbulence and flame interaction is believed to be purely kinematic. These two regimes correspond to thin reaction zone and corrugated flamelet regimes respectively. Turbulent flame speed in the present study is calculated from this approach regarding that the combustor is working under turbulent conditions.

1.2.3 Borghi - Peters diagram

The interaction between turbulent flow field and the flame front is classified using Borghi-Peters diagram through a number of dimensionless parameters. These are the turbulent Reynolds number (Re_t), Damköhler number (Da), and Karlovitz number (Ka). Reynolds number is the ratio of inertial forces to viscous forces. The region under Re_t=1 line is termed as laminar flames. Damköhler number plays an important role since strong time dependency of turbulent phenomena that is defined as the ratio of the characteristic flow time scale to the characteristic chemical reaction time. Combustion process is controlled by chemical kinetics, with decreasing Damköhler number (Da<1) corresponds to the stirred reactor zone while large Damköhler numbers (Da>>1) defines several regimes, which are called flamelet regimes. Furthermore, large Damköhler number refers to fast chemistry as the chemical time scale is smaller with respect to turbulent flow time scale. Finally, Karlovitz number defines the relation between the laminar flame thickness (δ_L) and the smallest

turbulent flow scale epitomized as Kolmogorov microscale (η). Borghi-Peters diagram and corresponding regime boundaries can be observed in Figure 1.1.

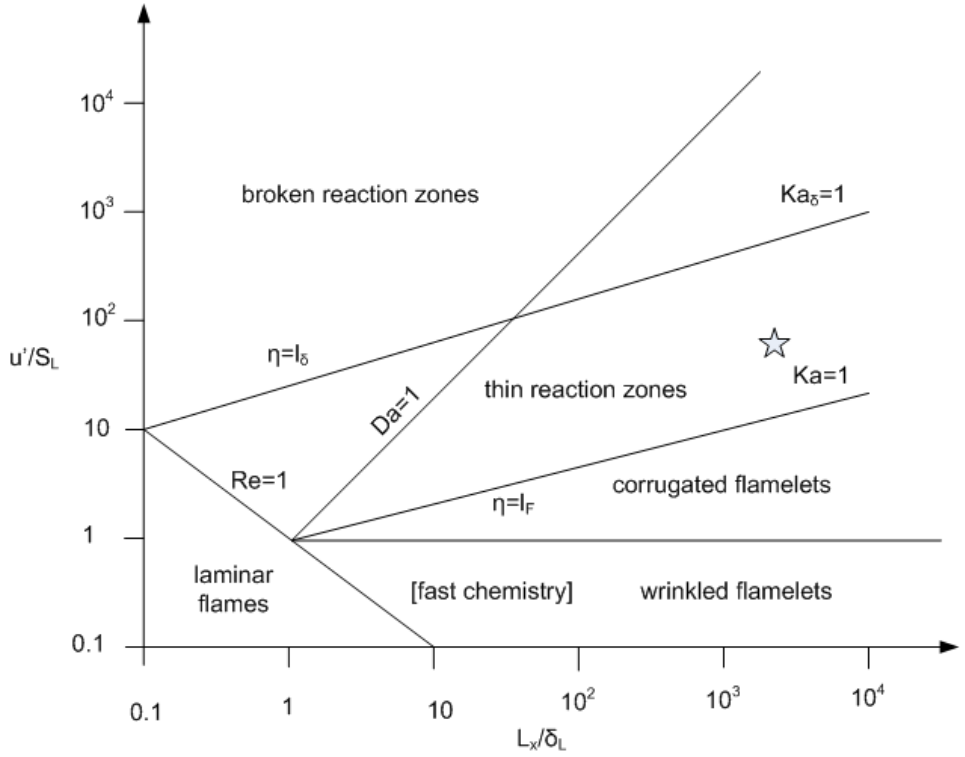

Figure 1.1 : Borghi-Peters regime diagram for premixed combustion (test condition indicated with a star symbol).

Corrugated and wrinkled flamelet regimes are restricted with Ka=1 line in the Borghi-Peters regime diagram. In these regimes interaction between flame front and the turbulent flow field is purely kinematic [12]. Wrinkled flame regime is similarly confined by the $\grave{u}/S_L$=1 line. Under this line laminar flame speed dominates the turbulent fluctuations. Therefore the thickness of the flame front is not altered by turbulence as the Kolmogorov eddies are so much larger than the laminar flame thickness. In the corrugated flamelet regime, flame front wrinkles more than the wrinkled flamelet regime since turbulent flame speed can be much higher than the laminar flame speed. In this regime "flame pockets" are produced by intense turbulence level nevertheless large Kolmogorov eddies still cannot diffuse into the reaction zone. On the other hand in the thickened flamelet regime, turbulent eddies are small enough to penetrate into the flame front, resulting an increase in heat diffusivity and a corresponding increase in flame thickness [13].

1.2.4 Swirling flames

Swirl stabilized premixed combustion is often used in internal combustion and gas turbine engines, furnaces, gasifiers and boilers to increase the heat and mass transfer. Flames in gas turbine combustors are often stabilized by passing the reactants from a swirler. When of sufficient strength, swirl produces large adverse pressure gradient in the streamwise direction, that leads to vortex breakdown and subsequent flow reversal. The resultant recirculation zone, carries hot combustion products and free radicals, which act as a stabilizing source for the flame, back towards the dump plane of the combustor.

Swirl stabilized combustors have substantial advantages in terms of improved combustion efficiency, better ignition stability, and reduced pollutant emissions. These benefits are believed to be the consequence of increased mixing rates due to enhanced turbulence levels [14].

1.2.4.1 Swirl number

Swirl number is defined to be the ratio of tangential momentum flux to axial momentum flux as per Eq. (1.1). Here, u_z is the axial mean velocity, u_θ the tangential mean velocity, and r denotes the radial coordinate. Note that this expression is simplified and excludes a pressure term [15].

$$S = \frac{\int_{R_i}^{R_0} \overline{u_z u_\theta} r^2 dr}{\int_{R_i}^{R_0} \overline{u_z^2} r dr} \tag{1.1}$$

Provided that axial and azimuthal velocities are uniform and the blades of the swirl vane are infinitely thin, the swirl number can be calculated by Eq. (1.2) [15].

$$S = \frac{2}{3}\left[\frac{1-(R_i/R_0)^3}{1-(R_i/R_0)^2}\right]\tan\theta \tag{1.2}$$

1.2.5 Image processing

1.2.5.1 Edge detection

Edge detection is a process which attempts to capture the significant properties of objects in the image as defined by Ziou and Tabbone [16]. With respect to the discontinuities in grey level image, characteristics of the image could be identified.

The most commonly used variations can be classified as discontinuities (step edges), local extreme (line edges) and edge crossings (junctions) inside the image [16] and they constitute necessary and sufficient conditions to define an image.

Since physical properties of a RGB image comprise depth, radiance and orientation of the objects, it has to be converted to grey-level in order to change these properties to one dimensional intensity distribution. Regarding to the intensity function, edges can be found from steps, lines and junctions. While steps generally occur between two regions having constant but different grey levels, lines occur between contacting images which are mutually illuminated objects. In spite of that, blurred and distorted images result noise thus suspicious edges. In addition to that gradual change in intensity causes problems as edge localization, false edges and missing real edges. Hence, an appropriate algorithm has to be chosen to deal with these kinds of problems.

In the open literature, there are numerous edge detection algorithms which are specialized with different types of edges. This section defines the most commonly used methods for edge detection starting with snake algorithm then gradient based algorithms. In addition to that, a comparison between snake and gradient based algorithms can be found in [17].

Snake algorithm

Active contour model, also called snake, could be another edge detection method which is known as an energy minimization method [18]. Snakes can be defined as splines that can move under the influence of internal (image) forces and external (curves computed from image data) forces. For initializing the snake algorithm, an ordinary shape has to be drawn previously as the algorithm does not capable of self-starting. Once the algorithm is started, internal forces try to shift the snake to the image features like lines and edges on the other hand; external forces try to move the snake to the local minimum positions. If an attempt to change the position of snake has made, snake will be replaced autonomously according to the energy minimization approach. Snake algorithm is widely used in medical imaging, line detection, single and multiple object tracking can be find in [19-22].

Prominent feature of snake algorithm comes from its energy minimization procedure which means any initial figure will fit to the edge of the given image by equalizing

the internal and external energies. However, depending on permanently search for closed object, snake algorithm does not give exact flame front position as combustion process may occurs in infinitesimal thin zone.

Gradient based algorithm

In contrast with the snake algorithm, edge detection methods were separated under two categories by Maini and Aggarwal, as gradient based and Laplacian based edge detection respectively [23]. While gradient based algorithms utilize the first derivative of the image in order to find the extremes, on the other hand, Laplacian based algorithms use the second derivative information to find the zero crossings for detecting edges. Most successfully used methods with their capability can be presented as Prewitt [24], Sobel [25] detectors which use local gradient operators however poor performance presented in case of blurred and noisy edges, Marr-Hildreth [26] is specialized since smoothing filter was proposed firstly within their paper and Canny improved existing edge detection algorithms, comparison of the detectors can be found in literature [27-29]. For further details in operators, reader should check [30].

In this thesis, special attentions focus on Canny edge detection algorithm since, its superior performance in edge detection. Thus, next section dedicated to Canny edge detection method.

Canny edge detection

As a Gaussian based algorithm, Canny use existing techniques and specialize them to improve his detector. Before Canny's work, Marr and Hildreth decided that Gaussian filter is the only operator which satisfies the uncertainty relation with both in spatial and frequency domains. As an optimal smoothing filter, Gaussian filter of different scales (σ) was applied to an image, then a set of different levels of smoothness were obtained [31]. To detect the edges second derivatives of the image must be calculated to find the zero crossings. Marr and Hildreth achieved this by using the Laplacian of a Gaussian (LOG) function as a filter [31]. Gaussian filter and Laplacian of Gaussian (LOG) can be seen from Equation 1.3 and Equation 1.4, respectively.

$$g(x,y) = \frac{1}{2\pi\sigma^2} e^{-(x^2+y^2/2\sigma^2)} \quad \textbf{(1.3)}$$

$$\nabla^2 g(x,y) = \frac{d^2}{dx^2} g(x,y) + \frac{d^2}{dy^2} g(x,y) = \frac{x^2 + y^2 - 2\sigma^2}{2\pi\sigma^6} e^{-(x^2+y^2/2\sigma^2)} \quad \textbf{(1.4)}$$

where σ represents standard deviation of the Gaussian filter. However, Marr-Hildreth algorithm gives poor response when the image has low signal to noise ratio (SNR). Canny improved some of the existing algorithms by reducing the error rate, good localization and having only one response to a single edge [32]. Good detection and good localization was achieved by increasing the SNR and closely marked point (by the operator) at the center of the true edge. Thus elimination of multiple responses was achieved by ignoring the behavior of the filter nearby the edge center, associated with the above criteria's. Canny's algorithm consist four main steps which are elaborated below;

- Smooth the image using a two dimensional Gaussian filter. Due to computational cost of a two dimensional Gaussian, x and y directions could be smoothed respectively.
- Take the gradient of the images. Gradients of the images founded separately as in the smoothing part.
- Non-maximal suppression. Edges will be mostly occurred at the maximum gradient point. When non-maximum suppression applied to an image, non-continuous and "wandered" edges will be dropped out.
- Edge thresholding. Canny's thresholding method is different than the others specializing with hysteresis. If a part of a contour has a higher value than the higher threshold, those points become immediately output, even if an entire connected segment of contour has partially lies above a low threshold. Similarly pixel value lower than the lower threshold is eliminated directly.

Further details pertaining to the mathematical method can be examined in [32].

2. EXPERIMENTAL SETUP

A fully premixed swirl stabilized combustor was built to study both flame front characteristics and the interaction between flame and flow, additionally validation of further numerical studies [33] experimental data is strongly needed, however; it is not scope of this thesis. Overall view of experimental setup is provided in figure 2.1. As the flame is stabilized just above the dump plane, quartz windows placed for optical access. Back plane was constructed from metal sheet and it has pressure and igniter ports. Above of all a nozzle is mounted to pressurize the combustion chamber. However, complexity of pressurized tests as need of cooling for quartz windows, intense agglomeration on quartz windows etc. reduces both the time and the repeatability of the experiments. Thus experiments are conducted at atmospheric conditions for this study by removing the top section.

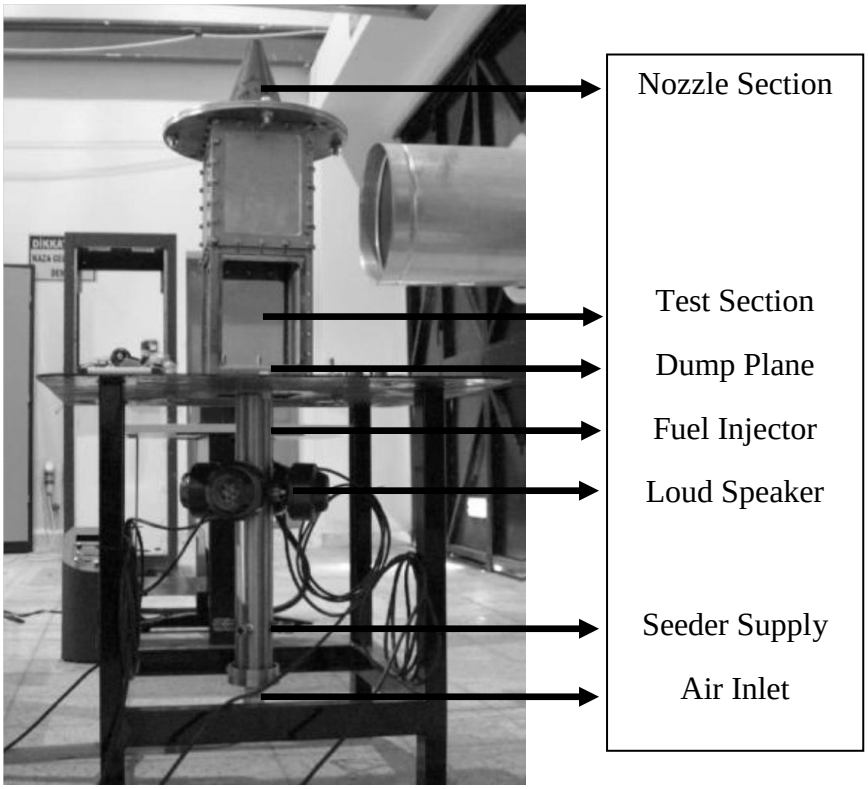

Figure 2.1 : Overall view of experimental setup.

2.1 Test Setup

Open flame configuration can be seen from figure 2.2. Through the delivery tube air flow has enough time to be straightened. Various holes were drilled to delivery tube for supply, measure and control the flow. Along the pipe, air supply connected at the bottom of the system above of it seeder supplying holes takes place, following that screw threaded holes for loudspeaker to modulate the flow (which is not used in this thesis), pressure transducer hole and lastly fuel injector hole lay on it. Pipe diameter is set to $70\,mm$. Flow rate is restricted to $60\,m^3/h$. For changing the experimental condition with respect to flow velocity, an area reducer system which has $50\,mm$ and $70\,mm$ of inner and outer diameter is manufactured. Thus, hollow rod can be positioned upper part of the delivery tube whenever it is necessary to change the experimental conditions.

Figure 2.2 : Test rig (Open flame configuration).

Flow field is inspected with 2D Particle Image Velocimetry (PIV) technique. This system is capable of measuring the velocity vector in two components. For visualization, a double cavity Nd:YAG laser operating at 532 nm wavelength is used as the light source. Sheet optics turn the laser line into a thin plane of approximately two millimeters in thickness. The imaging region is located above the dump plane. To record the PIV images two different CCD cameras with 1600 x 1200 and 1600 x 2480 resolution are used for separate experiments. While higher resolution camera

gives better images the other one provides more detail about the flow field. Note that, for the reliability of the velocity vectors, illumination plane and the camera axis must be mutually orthogonal. An optical interference filter centered at 532 nm wavelength with a bandwidth of 10 nm FWHM is used to restrain the natural emission of the flame in order to improve the signal to noise ratio. While calibrating the camera a target marked with a checkerboard pattern is placed parallel to the light sheet and pixel-wise resolution in either direction is adjusted. The illuminated flow area is approximately 150 mm x 240 mm in size. Correct seed density and the illumination power have to be adjusted for accurate PIV post-processing on the other hand; it does not have to be too dense to over-saturate pixels of the camera.

TiO_2 particles were chosen to seed the flow due to their high temperature resistance and being small enough (on the order of 100 nm) to follow the fluid. Before each experiment, high humidity inside the seeder drum is removed by simple heaters in order not to allow agglomeration within the test rig. This agglomeration would cause extensive glowing area that yields nearby pixels to loose their brightness relative to this area and consequently bad vectors appear in the calculations. Even if the solid particles are small enough, agglomeration has to be taken into consideration, thus in the late experiments liquid particles were used to seed to flow as this size is on the order of 2 μm in characteristic length. For this purpose a Laskin-nozzle type seeder were used to seed the flow. It produces fine oil mist in the observed field. Another significant benefit of the liquid particles can be presumed once they enter to combustion zone, they start burning and disappear by giving the flame front location precisely. Keeping in mind, they do not give any information about the product side of the flow thus it is not a good method for investigation of the flame-flow interaction within the recirculation zone.

2.2 Swirl Burner

Swirl vanes were classified into several types as conventional, tangential and low swirl vanes. In this study a conventional type swirl vane is used for the experiments. Top view of the swirl vane can be seen in figure 2.3. This kind of swirl vanes were designed with angled axial blades and an additional center body flame holder rod. As mentioned before, swirl vane and the dump plane, which also can be seen from

figure 2.3, constitute the swirl burner. This laboratory scale burner can be fired up to 30 kW of thermal power.

Figure 2.3 : Advanced structures.

Designed swirl vane has eight blades at an angle of 45° with respect to the oncoming flow. The inner and outer radii of the swirl vane blades are 20 mm and 50 mm respectively. The diameter of the center body is 20 mm. Noting that the swirl number, calculated from equation 2.1 as 0.74, includes the assumption of uniform axial and azimuthal velocities and infinitely thin swirl vane blades. Depending on the order of the swirl number it is named as moderate swirl vane.

$$S = \frac{2}{3}\left[\frac{1-(R_i/R_0)^3}{1-(R_i/R_0)^2}\right]\tan\varphi \qquad (2.1)$$

Methane is assumed to be fully premixed before entering to the swirler. The swirling reactant flow encounters a sudden expansion at the dump plane. Due to this swirling motion expanding flow slows down (due to conservation of angular momentum) pressure builds up and consequently a recirculation zone is established downstream of the dump plane which is instrumental in flame holding.

2.3 PIV Images

As outlined in section 2.1, flow field is inspected with PIV technique and at the test condition over than two hundred image pairs were acquired by selecting the inter-pulse time interval (Δt) around 30μs between consecutive images. For velocity measurement, observing the flow area from a distance gives satisfying results and measurements concern the whole measurement plain to get a general idea about the

illumination plane will be enough. However, investigation of flame characteristics shall be examined in detail as the order of the flame thickness is about 10^{-3} m. To achieve these necessities images are recorded with different zoom ratios and correlation window sizes, thus different time regretion values (Δt) for velocity and flame investigations. Details will be mentioned in subsequent sections.

For all experiments, inter-pulse time interval is selected as the particle in an interrogation window will move in order to one-fourth and one-tenth rules, which are defined as a particle in an interrogation window allowed to move one-fourth of the interrogation window with its maximum speed, analogously minimum allowable displacement must be one-tenth of the interrogation window size at the selected time interval. For example; if the interrogation window is selected as 32 x 32 pixels, then the displacement of the fastest particle must move 8 pixels on the contrary, slowest particle has to move 3.2 pixels (it must be round up to an integer) at a given flow speed. By estimating the flow speed and the displacement interval, an appropriate time interval can be selected.

2.4 Velocity Measurement Methodology

A widely used method for pre-processing the consecutive PIV images with a small infinitesimal time rate is known as the cross-correlation method. Particle image Velocimetry (PIV) technique is utilized to determine the velocity vector map on the illuminated plane from a double or multiple recorded image pairs [34].

Since several thousand vectors were calculated from every image pair, the necessary computational power is excessively high. For a given N x N interrogation window, N^4 calculations need to be done. Thus, Fast Fourier Transform (FFT) algorithm should be used for cross-correlation method. According to the correlation theorem, correlation between two functions in frequency space can be calculated by multiplying the complex conjugate parts of the Fourier transform of the first function and the Fourier transform of the second function. This method extremely accelerates the calculation.

Peak point of the correlation function which is calculated in frequency domain shows the mean displacement of the particles inside the interrogation window. Thus, a vector can be calculated from each correlation window, later than they can be

averaged. However, this method particularly in low signal/noise ratio case does not give exact solutions. As in this study, finding velocity vector calculations after averaging the correlation function is the optimal method to improve signal/noise ratio when seed density in flow area change drastically (Figure 2.4). In contradiction to the widely used method for resolving the velocity field by cross-correlating the images, average correlation method is used to determine the velocity vector map. Calculation method is represented in Figure 2.5. By using this method, there will not be wrong vector calculations wherein low signal to noise ratio regions due to light seed density.

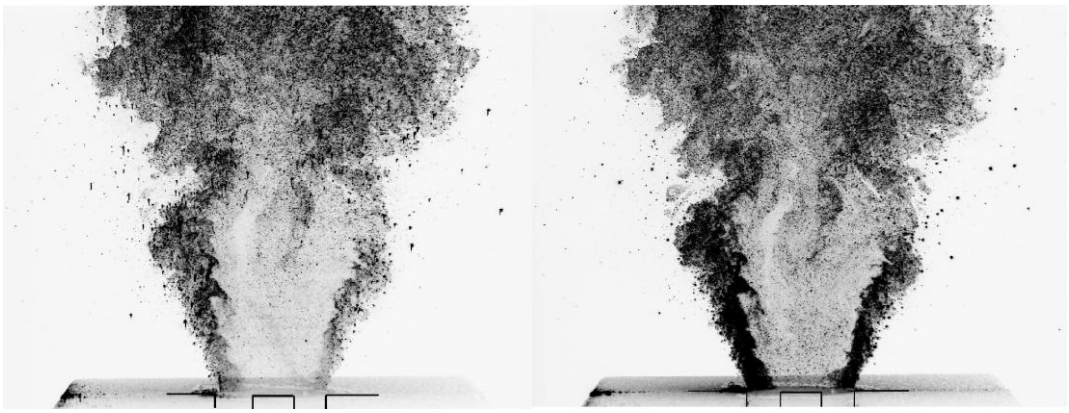

Frame A Frame B

Figure 2.4 : Inversed PIV images ($\Delta t = 30\ \mu s$).

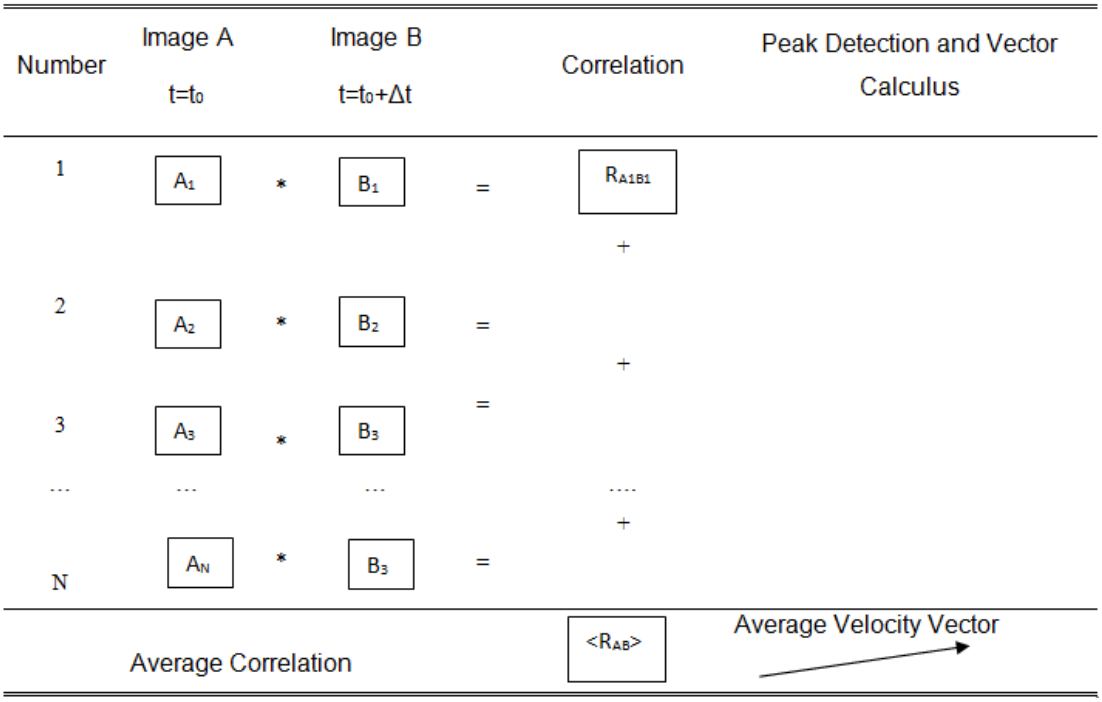

Figure 2.5 : Average correlation method.

2.4.1 Velocity measurement

For the velocity measurements, 276 image pairs were acquired with an inter-pulse time interval of $\Delta t=30\mu s$ between images, at the test conditions. Interrogation window is selected as 64 x 64 pixels, with a 50% overlapping in each direction yielding a spatial resolution of 4 mm. For some cases to detect the turbulent flame velocity interrogation window is set to 16 x 16 pixels, with 50% overlapping in each direction yielding a spatial resolution of 0.8 mm. In addition to that Δt is selected as $20\mu s$ for the second case in order not to get wrong vector calculations. In fact small difference in Δt does not gives bad vectors so it can also be selected as in the first case.

2.4.2 Flame characteristics measurement

Two image set were stored by selecting different Δt. First one is selected with the same configuration with velocity measurement but a smaller interrogation window (16 x 16 pixels). The second one is selected as the same interrogation window size with the first one but a lowered Δt value and zoomed camera condition are used.

Nevertheless, by the nature of swirling and reverse flows, velocity gradients changes from place to place, hence decreasing interrogation window sizes do not give accurate solutions for the whole field. Therefore; inter-pulse time interval has to be selected for the region of interest (in this situation: flame zone). While working with flame front characteristics velocity vectors which are away from the flame front will be called as bad vectors due to selected inter-pulse time interval was set for the velocity vectors placed at the flame front. This method corresponds to the second image set.

3. RESULTS & DISCUSSION

3.1 Preliminary Cold Flow Measurements

Prior to reacting flow measurements the structure of the cold flow is investigated with the help of particle image Velocimetry (PIV) technique in order to gain useful insight into the flowfield. In this measurement technique, the flowfield is seeded with small enough particles (such that they can follow the fluid) that scatter light. The flow entrained with seed particles is illuminated twice in quick succession and image pairs are recorded. Then motion of the seed particles are used to calculate the velocity field through spatial auto-correlation[34].

In this particular arrangement, TiO_2 particles were used to seed the flow, since these particles have a high melting point (particularly important for reacting flow cases), they often used in combustion application. However, in some cases oil is used to seed to flow, which will be discussed in further sections. A double cavity Nd:YAG laser was used as the light source. A cylindrical lens sheet optics arrangement was provides an approximately 2 mm light sheet that passes through the flowfield along with the diameter of the bluff body. The illuminated area is approximately 150 mm x 200 mm in size. The CCD camera used for imaging has 1200 x 1600 pixels resolution. Raw PIV images for a single double exposure are provided in Figure 3.1. Note that these images are color inverted for clarity. Time interval between these images is $30\mu s$.

Figure 3.1 : Inverted PIV Image (TiO_2).

A little more than two hundred image pairs were recorded and the resulting data was ensemble averaged in order to provide velocity uncertainties of approximately 2%. The field of view was split into interrogation regions of 32 x 32 pixels, with a 50% overlap, yielding a spatial resolution of 2.52 mm.

Ensemble averaged velocity vectors and vorticity strength of the cold flow are both provided in Figure 3.2. Note that the velocities are non-dimensionalized with the mean axial velocity at the delivery tube. Spatial coordinates are also non-dimensionalized with respect to the radius of the delivery tube. Location of the center body and the dump plane are marked in Figure 3.2. Jet discharge and entrainment of the ambient medium into the shear layer can be clearly seen. Furthermore two elliptically shaped counter rotating recirculation vortices can clearly be discerned from Figures 3.2 and 3.3. Reverse flow along the centerline of the combustor is also evident. These recirculation zones form due to the sudden expansion of the swirling flow at the dump plane. As the flow expands angular velocity of the swirling motion slows down due to conservation of angular momentum resulting in the buildup of static pressure along the centerline, which provides that the swirl is of sufficient strength. Finally this phenomena yields a reverse flow and the establishment of a central recirculation zone just above the dump plane is ensured. This main recirculation region entraps hot combustion products and free radicals (in reacting flow case). These effects are crucial flow sutructure in flame holding. Furthermore due to sudden expansion there are secondary recirculation zone formed above the dump plane. These flow features can also be seen in Figure. 3.3.

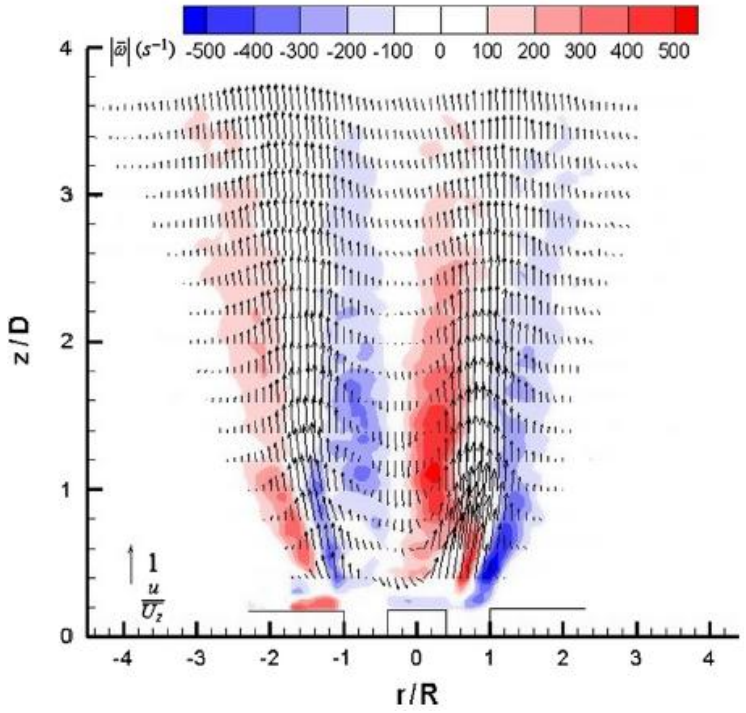

Figure 3.2 : Mean velocity vectors and out of plane vorticity magnitude (S = 0.74, Re_{Dh} = 19 400 and $\dot{Q}_{air}$=16.7 l/s)

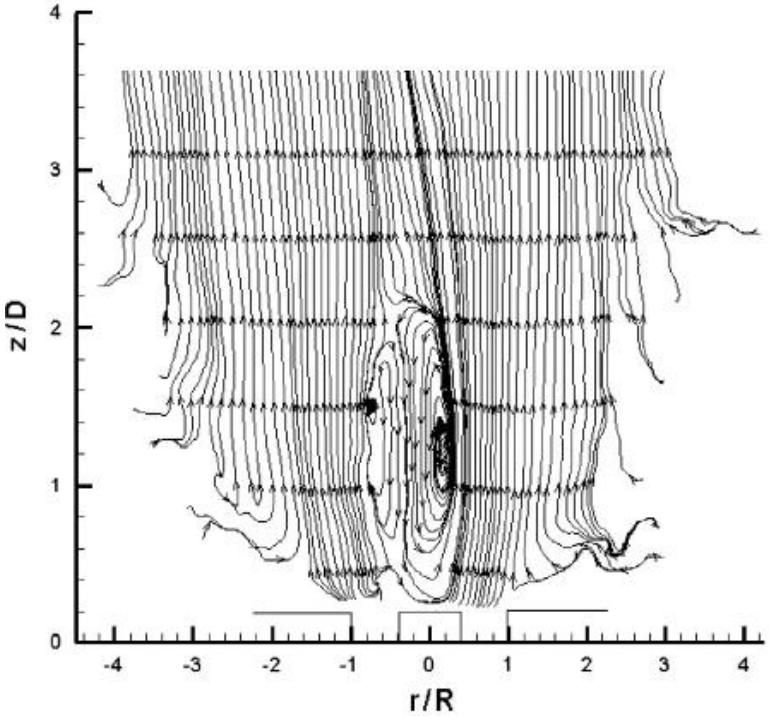

Figure 3.3 : Streamlines and recirculation zones. (S = 0.74, Re_{Dh} = 19 400 and $\dot{Q}_{air}$=16.7 l/s)

3.2 Reacting Flow Measurements

At the test condition 276 image pairs were acquired with an inter-pulse time interval Δt = 30μs between images. A 16x16 pixel interrogation window with %50 overlap was used which produces velocity vectors on every fourth pixel, corresponding to a spatial resolution of 0.8 mm in either direction. Average correlation method was chosen since it is a convenient method when the seed particle density changes dramatically within the flow field. Average correlation method correlates each interrogation window one by one at the same point and sums up all the peaks adopted from these interrogation windows to find a velocity vector corresponding to this interrogation area. This operation is iterated for every window. Instantaneous PIV image couple, which is used for vector calculus can be seen from Figure 3.4 and Figure 3.5 for both particle types.

A substantial observation between cold and reacting PIV images can be made according to TiO_2 particle density distribution. It is known that PIV images from the tracer particles for PIV measurements on combustion field show changes in number density of particles from unburnt to burnt regions due to gas thermal expansion [35]. Hence, there is a possibility to determine flame front boundary from the PIV images. In the cold flow case (Figure 3.1), a regular seed distribution can be observed, however in reacting flow case (Figure 3.4) distribution of seeding particles change with respect to flame front location and fluctuations, causing faster particle displacement in burned side. Thus, different velocity distribution between burned and unburnt side occur due to increased heat at the products side.

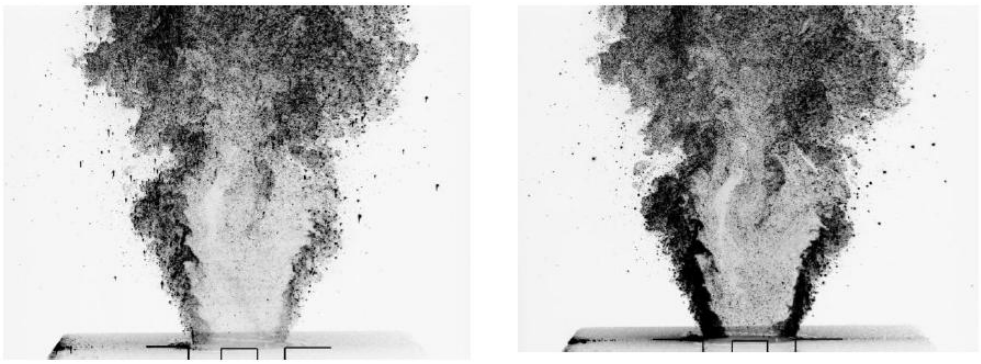

Figure 3.4 : Inversed PIV images (TiO_2 particles).

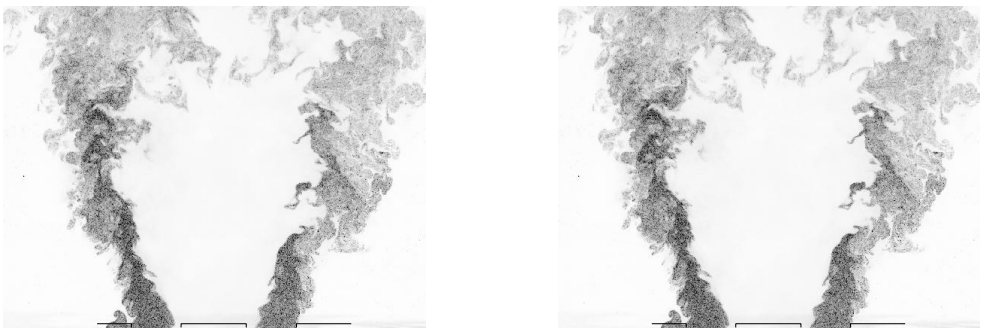

Figure 3.5 : Inversed PIV images (Oil particles).

3.2.1 Location of the flame front

By the nature of swirling flows, flame can be stabilized on three locations; outer shear layer (OSL), inner shear layer (ISL) and by vortex breakdown bubble (VBB)[36]. In the present case flame stabilizes at inner shear layer created by center body flame holder as in Figure 3.6.

Figure 3.6 : Visible flame front and dump plane.

3.2.2 Flow characteristics

Vorticity structure with non-dimensionalized vectors can be seen from Figure 3.6. One must note that opposite flow directions in measurements caused by different test times, during these times swirl burner may be rotated. Also expected behavior of the flow along diameter should be symmetric, however; small run off in the direction of the laser cause this kind of inclining. The behavior is caused by the three dimensionality of the flow.

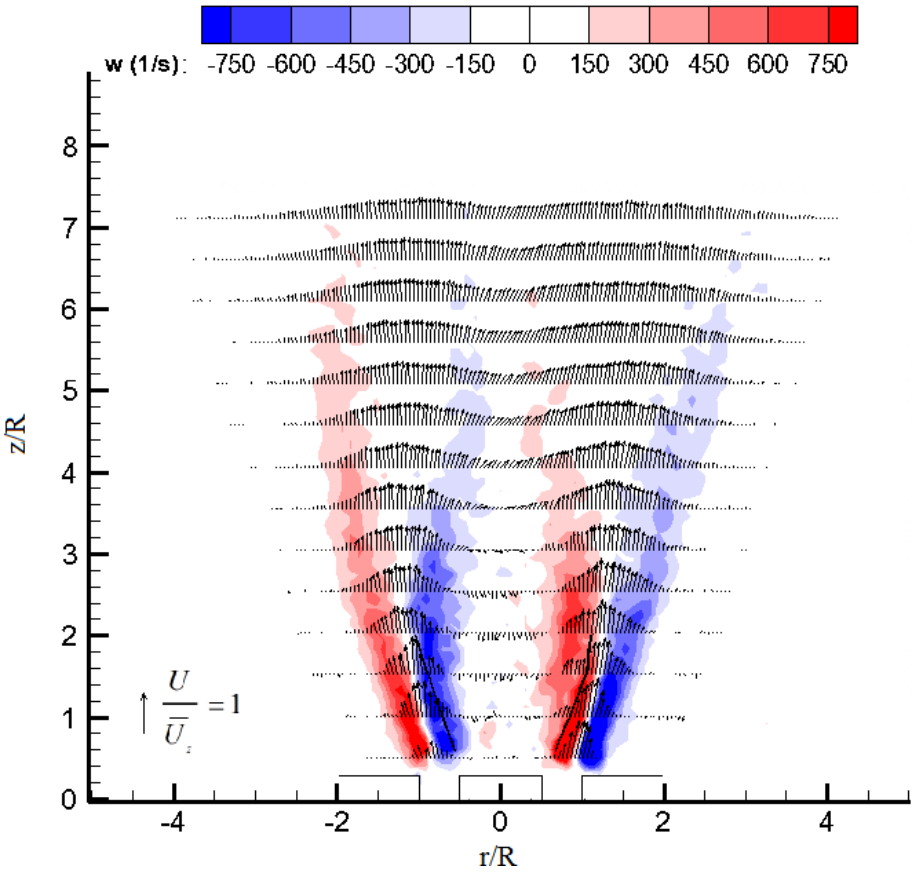

Figure 3.7 : Mean velocity vectors and out of plane vorticity magnitude of the reacting flow and flame front created by ISL over dump plane (TiO_2 particle).

A careful investigation of the velocity field and the image of the flame reveal that the structure of the flame near the dump plane corresponds closely to the features of the non-reacting flowfield. The flame is clearly seen to stabilize at the edge of the inner recirculation region. This observation hints to the resemblance of reacting and non-reacting flow structures. When the flow reaches to the dump plane, it expands due to low pressure. A re-circulation zone is established over the center body flame holder, which is called as the main re-circulation zone and at the edges of the dump plane there are secondary re-circulation zones that are much weaker than the main re-circulation zone. As one can readily observe the main re-circulation zone from the ISL, mixes the fresh reactants with intermediate combustion products, while inner flame front preheats the mixture steadily.

3.2.3 Post-processing for flame front detection

PIV images are processed to recover the flame front location separating the reactants and the products. As mentioned in experimental setup chapter, two different seeding particles are used in order to define flame front. While TiO_2 particles resistant to temperature and combustion, oil particles tend to burn whenever oil reaches to the flame front thus using different image processing algorithms is crucial. As in Figure 3.4 and Figure 3.5, gradient change at the flame front can be observed with naked eye, however distinct gradient change by using oil particle result an easy method for flame front detection.

3.2.3.1 Using TiO_2 particles

By using TiO_2 particles, Mie images were summed up to find the average scattering image and histogram of this average image was plotted to enhance image properties by both thresholding the gray image and also by adding Gaussian blur etc. Note that while fine smoothing suppresses the noise, excessive smoothing on the other hand destroys the image structure [37]. To focus on the expected flame edges area, a binary mask with ones and zeros was applied to the image where ones correspond to inside of the area. After these steps, the average Mie image was ready for edge detection. Prewitt and Canny methods were tested to determine the edges; nevertheless Canny algorithm yields better results at all. Hereafter, results which differ depending on seeding type will be indicated.

3.2.3.2 Using oil particles

With the oil used experiments, Mie images include information only at the unburned parts of the flow on the contrary flame contour and flame wrinkling can be observed distinctly even with a quick look in Mie images. The algorithm, which is used in image detection by using TiO_2 particle, is changed in order to deal with every single image. First of all original image was processed to suppress the background effects like dump plane surface. For this step, brightness of the image is stretched and adjusted according to the existing methods defined in MATLAB. After image is turned to gray-scale, as a standard procedure, Gaussian blur is added to the image by selecting $\sigma = 8$ and a kernel with 4 x 4 pixels. Note that other filters like Median and Wiener filters does not give good solutions for our case as their highly edge

preserving methods gives noisy signals for edge detection. Beside of that, edges are tried to be found only at the flame front thus Gaussian filter gives better result. Then, image is turned to binary image for edge detection. The resulting gray-scale image altered to binary image for the ease of image detection. After then, Canny edge detection algorithm applied to the binary image and only one pixel thick line response taken due to specialty of Canny's algorithm. After then, a binary mask with ones and zeros was applied to the image where ones correspond to inside of the area to focus on the expected flame edges area. This mask is applied after edges are detected as the physical boundary of a given masked image is defined as an edge according to the Canny's algorithm. As a last step, edge elimination according to the length of the spline element is set to 50 pixels long. This step is defined to eliminate the smaller wrong edges out of the flame front position. However, a longer pixel size may distort the original edges which can be defined disconnected due to edge detection algorithm. Resulted instantaneous flame front and wrinkles can be seen in Figure 3.8. One thing must be noted that, dump plane is placed just at the lower end of the image, however for the visibility of the dump plane and flame front position with respect to dump plane it is placed twelve pixels inside of the figure. Further details of the image processing steps can be found in Appendix 1. Note that, edges are perfectly continuous; however zoom out view to the flame front edges may cause loss in pixel property caused by optical illusion as the width of the flame front respesented with a single pixel.

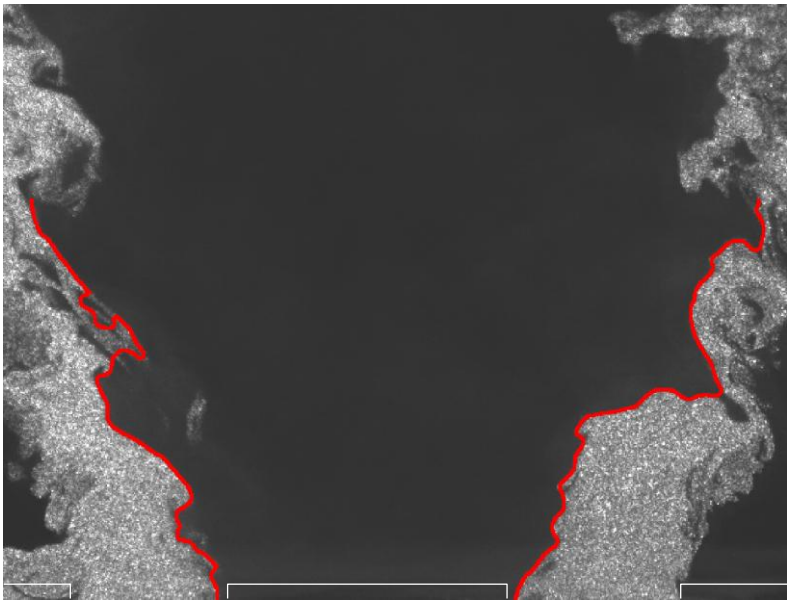

Figure 3.8 : Instantaneous flame front on PIV image (Oil particle).

3.2.4 Turbulent flame speed

As a consequence of Damköhler's study (1940)[38], having a turbulent flow condition instead of his Bunsen burner gives us directly the burning velocity from the PIV images that are provided in Figure 10. The turbulent flame front was expected to propagate with that burning velocity relative to the flow field. Along th e flame front turbulent flame speed calculated from equation 3.1. Note that turbulent flame speed was non-dimensionalized by the laminar flame speed. Laminar flame speed is calculated from the GRI 3.0 [39], it is found to be 0.4 m/s using CANTERA software [40].

$$\frac{S_T}{S_L} = \frac{A_T}{A} \tag{3.1}$$

Damköhler define this phenomena with equation 3.1, another result from this equation can be the analyses of the turbulent area fluctuations. From the equality, turbulent flame fluctuation is directly related with the turbulent burning velocity. From this point of aspect it is validated that increase in burning velocity is provided by flame front wrinkling that cause increase in flame area.

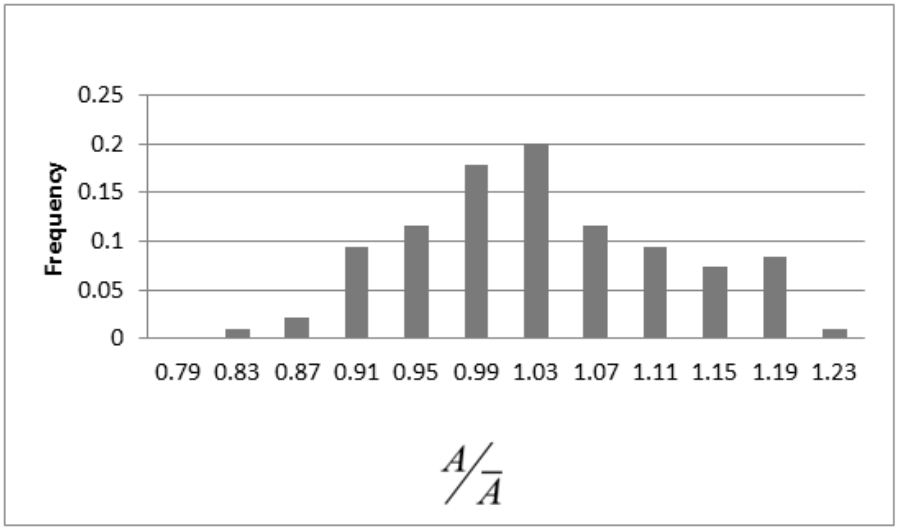

Figure 3.9 : Histogram of the instantenious flame front area (non-dimensionalized with respect to the time average value).

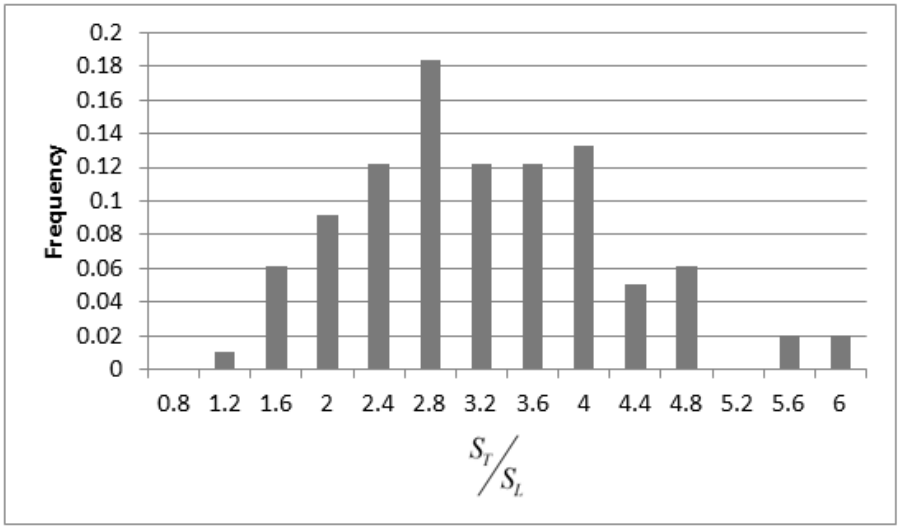

Figure 3.10 : Histogram of the burning velocities at an instantenious flame front.

As can be seen from Figure 3.9, instantaneous flame front areas are closer to average flame front areas around a standart deviation, though increasing scattering distribution around the average shows that flame front is wrinkling to enhance the combustion by turbulence. Similar distribution as flame front areas, as Damköhler's definition on turbulent burning velocity, shows a similary distribution as in flame front fluctuations. The probability density function appears to have a Gaussian shape.

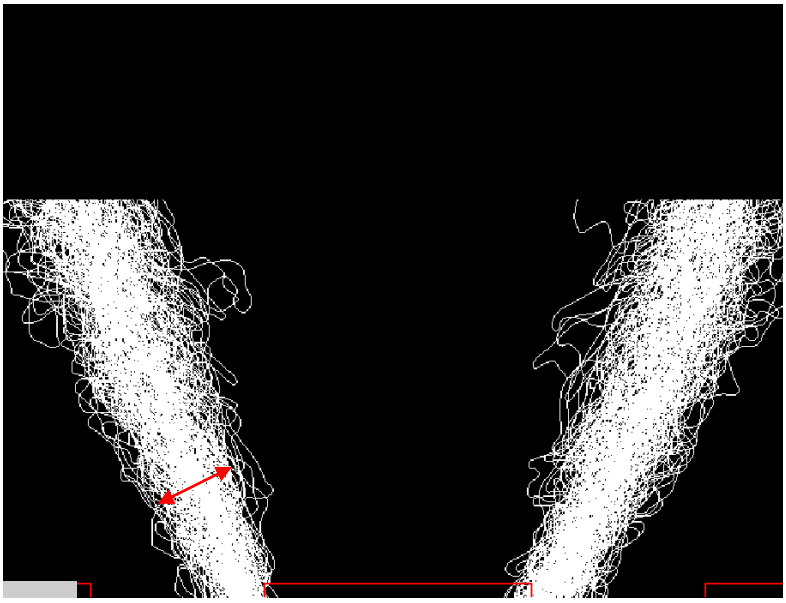

Figure 3.11 : Flame brush thickness(Length of the red arrow corresponds to 0.7mm).

Flame brush thickness can be described as the distance from the mean flame front that instantenious flame realizations can reach[41]. As an early method, G-equation is used to model the flame brush thickness to give a prediction of the flame front locations by dividing the burned and unburnt side of a given domain for numerical

analysis. Today's practical Computational Fluid Dynamics(CFD) applications such as Reynolds Averaged Navier-Stokes (RANS) and Large Eddy Simulation (LES) use a statistical averaged or filtered flame fronts to track the flame fronts. Thus flame brush thickness is one of the important parameter to resolve the critical lengthscales at the flame fronts in simulations.

In figure 3.11, flame brush thickness at the root section correspond to 0.5 mm and it tends to grow as the distance of the flame high increased. Even if the flame brush thickness change from place to place, order of the flame brush thickness match with respect to open literature in studied flame configuration.

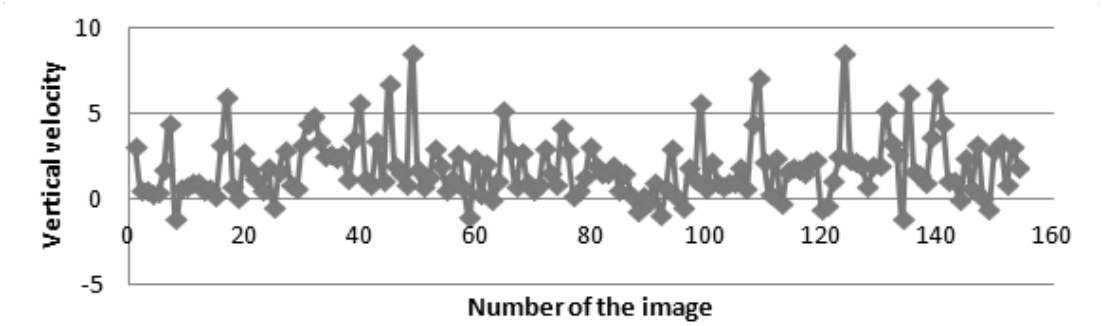

Figure 3.12 : Phase plot of vertical velocity.

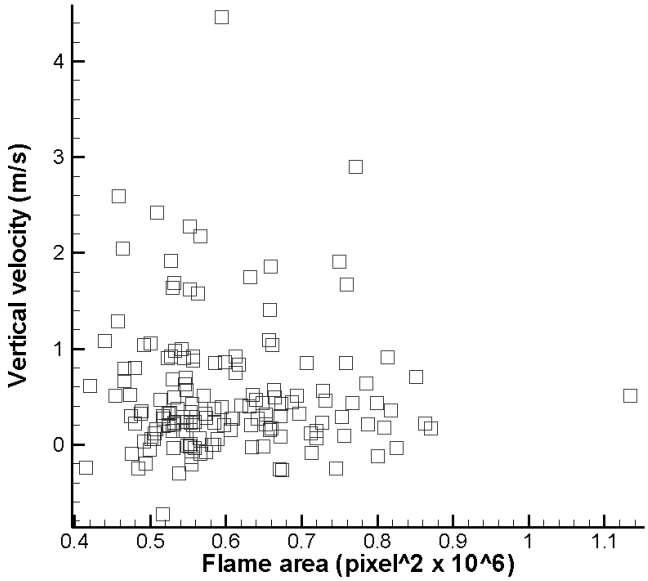

Figure 3.13 : Phase plot of vertical velocity versus flame areas.

According to phase plot of the vertical velocity as shown in figure 3.12, a dominant phase could not be observed however, this does not restrict the existance of the swirling motion oscillations. Similarly, vertical velocity and the flame areas does not have a comman pattern to define the precessing motion at the vertical cross-section plane as can be seen from figure 3.13.

4. CONCLUSIONS AND RECOMMENDATIONS

An atmospheric, open flame configuration test rig was established in order to reveal flame front characteristics and subsidiary investigation was focused on interaction between flame front and turbulent flow. Stability of the flame was inspected by comparing cold and reacting flow structure. At the studied configuration, a wedge shaped flame stabilizes on top of the center body flame holder in connection with inner shear layer (ISL).

Preliminary works on cold flow investigation results two recirculation regions which can be named as inner and outer recirculation regions. Inside the inner recirculation region adverse pressure gradient occur due to sudden expansion of the oncoming flow creating a reserve flow over the center body flame holder. Beside of that a weak recirculation region occurs at the edge of the dump plane due to interaction of the swirling flow with the stagnant air out of the investigated region. Both recirculation zones are responsible for feeding hot products back into the flame root. Thus, reactants are warmed up and mixed with intermediate products before completely burned. Comparing with the literature recirculated mass flow increase, with increased swirl. In essence of the matter, combustion stability and efficiency increased by using a swirl burner system. Comparatively with the reacting flow case by using TiO_2 particle, a similar flow structure was observed. Besides at the burnt side particle density decreases due to thermal expansion in this region.

For the investigation of flame front characteristics, an image-processing algorithm was composed in MATLAB to detect the flame front. They were determined by Canny edge detection algorithm using PIV images. TiO_2 and oil particles were used separately to obtain PIV images and they result different outcomes due to different gradient changes. Specifically PIV images by using oil particles were selected for processing as Canny yields better results in this case.

From the resulted flame fronts, which were obtained from image processing, were processed further more to calculate the mean flame front area and instantaneous flame front areas to get an insight on turbulent burning velocity. In the light of

Damköhler's definition by knowing flame area ratio and the laminar burning velocity, turbulent burning velocity were revealed and it was put out that increased flame area, by forming wrinkling at the flame front, directly increase the turbulent flame speed.

One thing must be noted that, decreasing the interrogation window up to 16 x 16 pixels when velocity vector calculation with PIV, user must observe the displacement of the particles in order not to get bad vectors in the observed area. Aside from that observation, investigated area can be narrowed further which cause an increase in spatial resolution, therefore the results with an increased interrogation window size could give increased number of successful velocity vectors. However, this method could not give the whole area investigation.

At the vertical cross-section, flame front does not have a comman pattern to define a precessing motion.

4.1 Further Works

Further works may concentrate on;

- Flame front fluctuation phenomena with respect to vorticity and strain rate on the flame front shall be elaborated in order to expand the interaction behavior.
- Along with PIV measurements, OH/CH chemiluminescence imaging can be performed in order to more precisely recover the flame behavior. This method also could verify the flame front characteristics, which was obtained by PIV images in the thesis.
- Moreover, interaction between swirl stabilized flame and acoustic waves shall also be investigated in detail.

REFERENCES

[1] **Url-1** <http://www.chevron.com/globalissues/energysupplydemand/>, date retrieved 15.04.2014.

[2] **Ateshkadi, A., McDonell, V. G., & Samuelsen, G. S.** (2000). Lean blowout model for a spray-fired swirl-stabilized combustor. *Proceedings of the Combustion Institute*, ***28*(1)**, 1281-1288.

[3] **Smyth, K. C., Miller, J. H., Dorfman, R. C., Mallard, W. G., & Santoro, R. J.** (1985). Soot inception in a methane/air diffusion flame as characterized by detailed species profiles. *Combustion and Flame*, ***62*(2)**, 157-181.

[4] **Yamashita, H., Shimada, M., & Takeno, T.** (1996). A numerical study on flame stability at the transition point of jet diffusion flames. In *Symposium (International) on Combustion*, Vol. **26**, No. 1, pp. 27-34.

[5] **Smooke, M. D., McEnally, C. S., Pfefferle, L. D., Hall, R. J., & Colket, M. B.** (1999). Computational and experimental study of soot formation in a coflow, laminar diffusion flame. *Combustion and Flame*, ***117*(1)**, 117-139.

[6] **De Ris, J. N.** (1969). Spread of a laminar diffusion flame. In*Symposium (International) on Combustion*. Vol. **12**, No. 1, pp. 241-252. Elsevier.

[7] **Johnson, M. R., Littlejohn, D., Nazeer, W. A., Smith, K. O., & Cheng, R. K.** (2005). A comparison of the flowfields and emissions of high-swirl injectors and low-swirl injectors for lean premixed gas turbines. *Proceedings of the Combustion Institute*, ***30*(2)**, 2867-2874.

[8] **Schefer, R. W.** (2003). Hydrogen enrichment for improved lean flame stability. *International Journal of Hydrogen Energy*, ***28*(10)**, 1131-1141.

[9] **Halter, F., Chauveau, C., & Gökalp, I.** (2007). Characterization of the effects of hydrogen addition in premixed methane/air flames. *International Journal of Hydrogen Energy*, ***32*(13)**, 2585-2592.

[10]**Tuncer O., Acharya S., Uhm J. H.** (2009). Dynamics NOx and Flashback Characteristics of Confined Premixed Hydrogen Enriched Flames. International Journal of Hydrogen Energy, **Vol. 34**, p. 496-506.

[11]**Damköhler, G.** (1940). Der Einfluss der Turbulenz auf die Flammengeschwindigkeit in Gasgemischen. *Z. Elektrochem*, 46, 601-652.

[12] **Siewert, P.,** (2006). "Flame front characteristics of turbulent lean premixed methane/air flames at high-pressure". Doctoral dissertation, Diss. ETH: 16369, Zurich.

[13] **Zimont, V.** (1979). Theory of turbulent combustion of homogenous fuel mixture at high Reynolds numbers. *Fizika Gorenyia i Vzryva*. **15**, 23-32.

[14] **Huang Y., Sung H., Hsieh S., Yang V.** (2003). Large eddy simulation of combustion dynamics of lean premixed swirl stabilized combustor. *Journal of Power and Propulsion*. **19**, 782–794,.

[15] **Gupta AK, Lilley DG, Syred N.** Swirl flows. Abacus Press. 1984.

[16] **Ziou, D., & Tabbone, S.** (1998). Edge detection techniques-an overview. *Pattern Recognition and Image Analysis C/C of Raspoznavaniye Obrazov I Analiz Izobrazhenii*, ***8***, 537-559.

[17] **Kimmel, R., & Bruckstein, A. M.** (2003). Regularized Laplacian zero crossings as optimal edge integrators. *International Journal of Computer Vision*, ***53*****(3)**, 225-243.

[18] **Kass, M., Witkin, A., & Terzopoulos, D.** (1988). Snakes: Active contour models. *International journal of computer vision*, ***1*****(4)**, 321-331.

[19] **Kang D. J., Choi J. W, Kweon I. S.** (1996). Finding and tracking road lanes using line-snakes, Proceedings of Conference on Intelligent Vehicle, , pp. 189–194, Japan.

[20] **Terzopoulos D., Szeliski R.** (1992). Tracking with Kalman Snakes, in: A. Blake, A. Yuille (Eds.), Active Vision, Artificial Intelligence, MIT press, Cambridge, MA, , pp. 3–20.

[21] **Xu C., Prince, J. L.** (1998). Snakes, shapes, and GVF, IEEE Transactions on Image Processing, 359–369.

[22] **Wang, Y., Teoh, E. K., Shen, D.** (2004). Lane detection and tracking using B-Snake. *Image and Vision computing*, ***22*****(4)**, 269-280.

[23] **Maini, R., Aggarwal, H.** (2009). Study and comparison of various image edge detection techniques, *International Journal of Image Processing*, **3(1)**, 1-11.

[24] **Prewitt, J. M.** (1970). Object enhancement and extraction. *Picture processing and Psychopictorics*, ***10*****(1)**, 15-19.

[25] **Kanopoulos, N., Vasanthavada, N., & Baker, R. L.** (1988). Design of an image edge detection filter using the Sobel operator. *Solid-State Circuits, IEEE Journal of*, *23*(2), 358-367.

[26] **Marr, D., & Hildreth, E.** (1980). Theory of edge detection. *Proceedings of the Royal Society of London. Series B. Biological Sciences*, *207*(1167), 187-217.

[27] **Zhang, R., Zhao, G., & Su, L.** (2005). A new edge detection method in image processing. In *Communications and Information Technology, 2005. ISCIT 2005. IEEE International Symposium on*. Vol. **1**, pp. 445-448. IEEE.

[28] **Nadernejad, E., Sharifzadeh, S., & Hassanpour, H.** (2008). Edge detection techniques: evaluations and comparisons. *Applied Mathematical Sciences*, ***2*****(31)**, 1507-1520.

[29] **Haralick, R. M.** (1984). Digital step edges from zero crossing of second directional derivatives. *Pattern Analysis and Machine Intelligence, IEEE Transactions on*, (1), 58-68.

[30] **Jain, R., Kasturi, R., & Schunck, B. G.** (1995). *Machine vision* (Vol. 5). New York: McGraw-Hill.

[31] **Basu, M.** (2002). Gaussian-based edge-detection methods-a survey. *IEEE Transactions on Systems, Man, and Cybernetics, Part C*, ***32*****(3)**, 252-260.

[32] **Canny, J.** (1986). A computational approach to edge detection. *Pattern Analysis and Machine Intelligence, IEEE Transactions on*, **(6)**, 679-698.

[33] **Tuncer, O., & Kaynaroglu, B.** (2014). Experimental and numerical investigation of a swirl-stabilized premixed methane/air flame. *Aircraft Engineering and Aerospace Technology*, **86(3)**, 215-224.

[34] **Raffel, M., Willert, C., Wereley, S., Kompenhans, J.** (2007) Particle Image Velocimetry, A Practical Guide, Second Edition, Springer-Verlag, Berlin, Germany.

[35] **Tachibana, S., Zimmer, L., & Suzuki, K.** (2004). Flame front detection and dynamics using PIV in a turbulent premixed flame. In *12th International Symposium on Applications of Laser Techniques to Fluid Mechanics*.

[36] **Zhang, Q., Shanbhogue, S. J., Shreekrishna, Lieuwen, T., & O'Connor, J.** (2011). Strain characteristics near the flame attachment point in a swirling flow. *Combustion Science and Technology*. ***183*****(7)**, 665-685.

[37] **Ziou, D., Tabbone, S. (**1998). Edge detection techniques-an overview. *Pattern Recognition and Image Anaylsis C/C of Raspoznavaniye Obrazov I Analiz Izobrazhenii*, ***8***, 537-559.

[38] **Damköhler, G.** (1940). Der Einfluss der Turbulenz auf die Flammengeschwindigkeit in Gasgemischen. *Z. Elektrochem*, **46**, 601-652.

[39] **Url - 2 Smith, G. P., Golden, D. M., Frenklach, M., Moriarty, N. W., Eiteneer, B., Goldenberg, M., Bowman, C. T., Hanson, R. K., Song, S., Gardiner, W. C., Lissianski, Jr. V. V., Qin, Z.,** (n. d.). Date retrieved 15.08.2013,
adress : http://www.me.berkeley.edu/gri_mech/

[40] **Url - 3 Goodwin, D. G.,** (2001-2005). Cantera. Date retrieved 15.08.2013, address: http://www.cantera.org.

[41] **Knudsen, E., Kurenkov, O., Kim, S., Oberlack, M., & Pitsch, H.** (2006). Modeling flame brush thickness in premixed turbulent combustion. In *Proceedings of the Summer Program* (p. 299).

APPENDICES

APPENDIX A: Flowchart and Image Processing Algorithm Steps

APPENDIX A

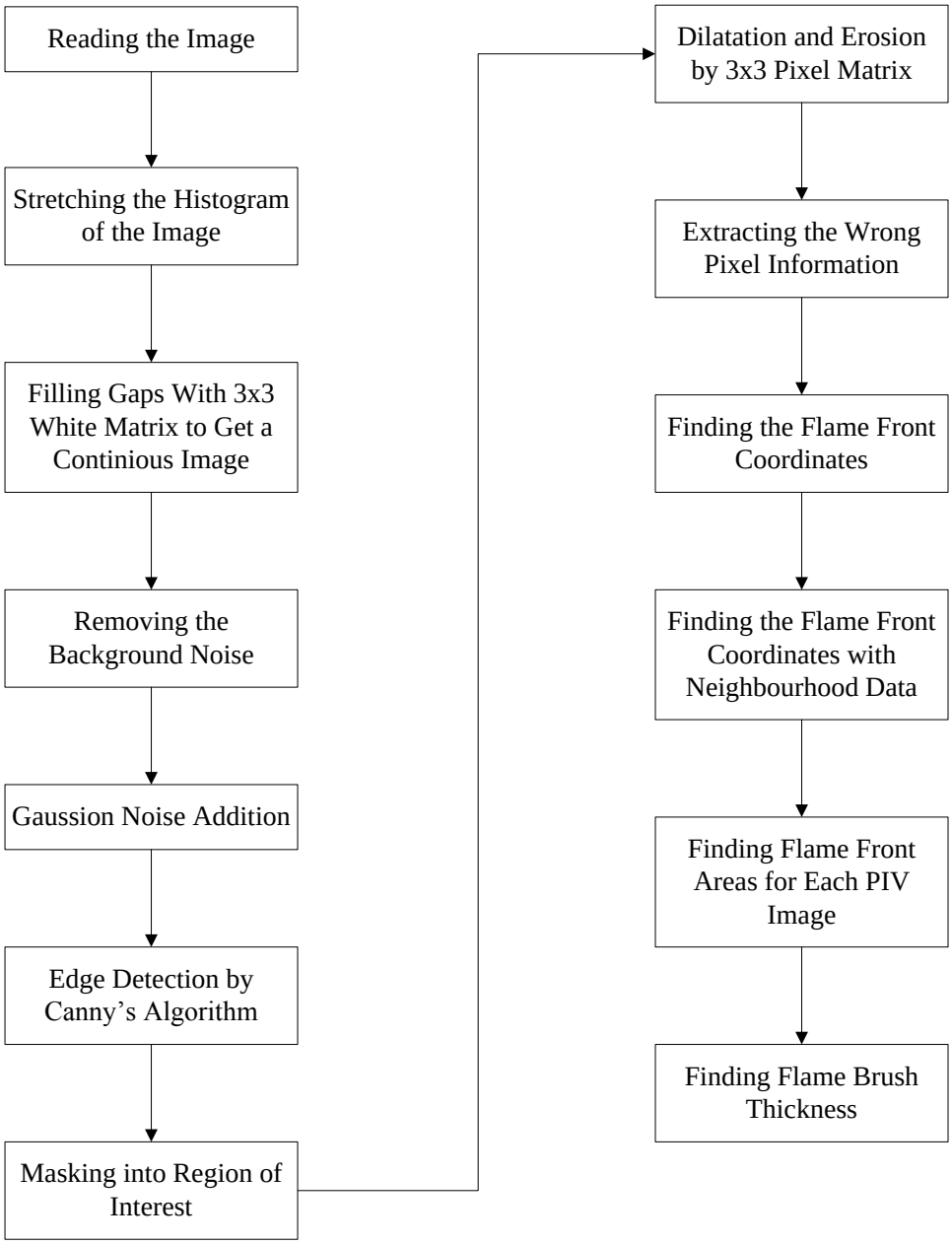

Figure A.1 : Flowchart for image process

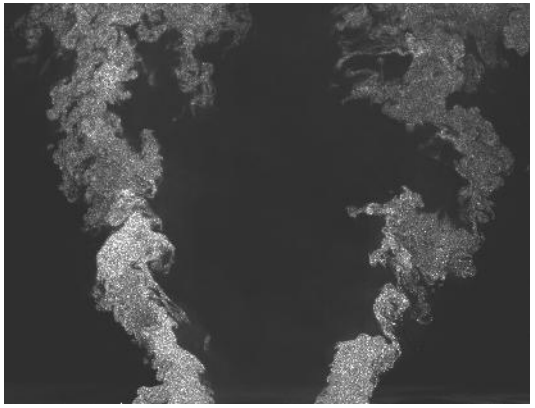

a. Original Image

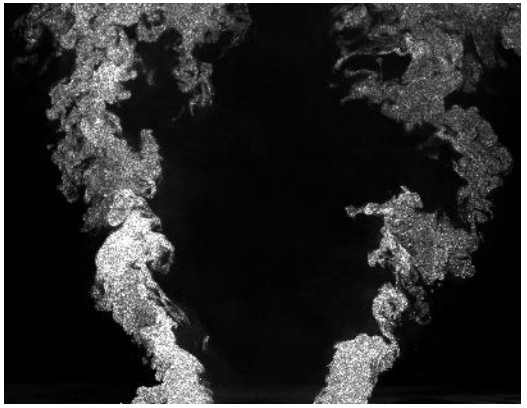

b. Streched Image

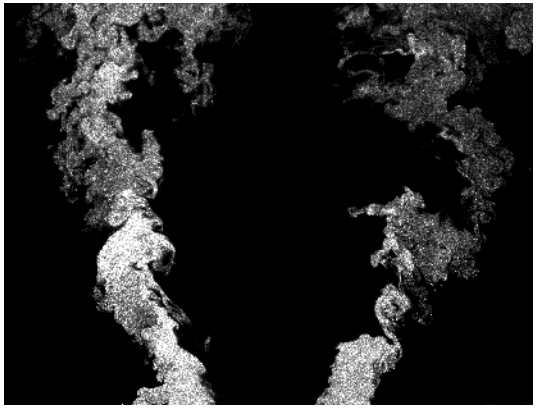

c. Brightness adjustment

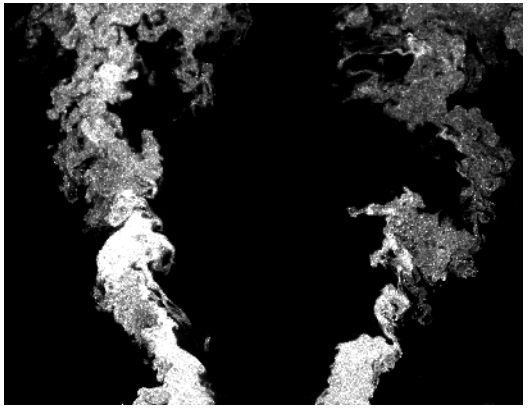

d. Dilated and eroded image

Figure A.2 : Image processing (Step 1).

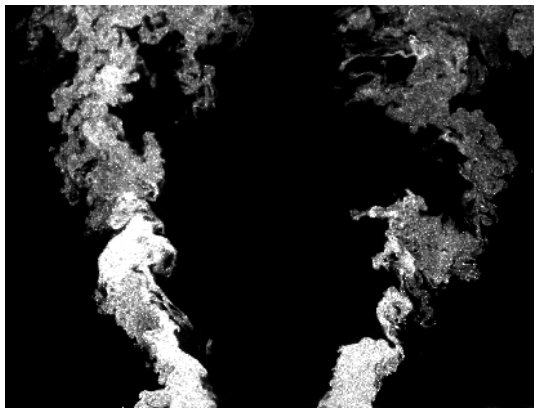

a. Dilated and eroded image

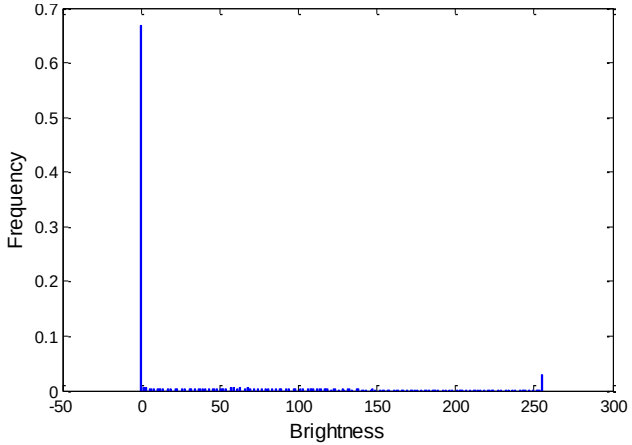

b. Histogram of the image at left

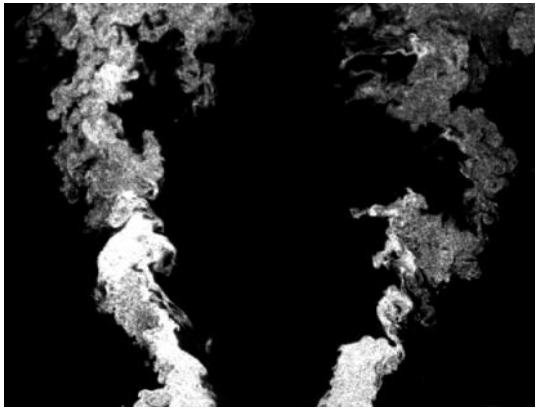

c. Gaussian filter ($\sigma = 8$)

d. Binarization after Gaussian filter

Figure A.3 : Image processing (Step 2).

a. Canny"s algorithm applied to binary image

b. Mask applied to region of interest

Figure A.4 : Image processing (Step 3).

a. Mask applied to region of interest

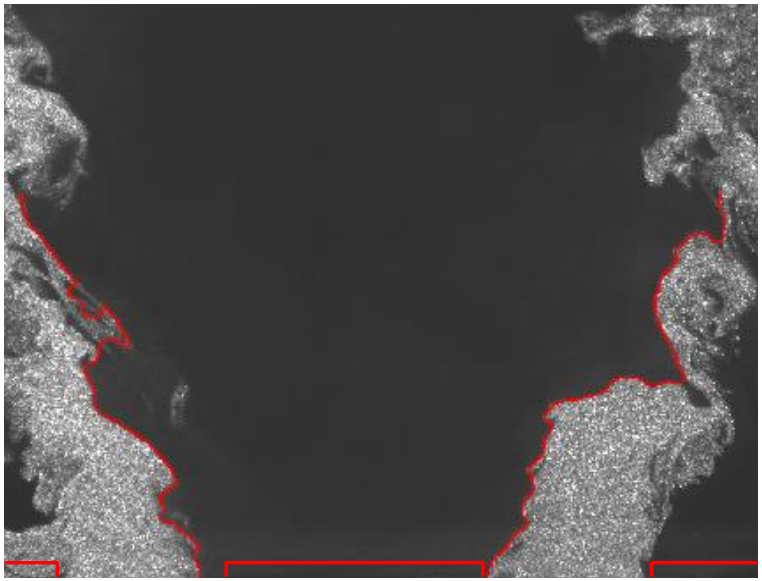

b. Line elemination according to the length and final result on PIV image

Figure A.5 : Image processing (Step 4).

CURRICULUM VITAE

Name Surname: Bertan Kaynaroğlu

Place and Date of Birth: Istanbul / 16.03.1989

E-Mail: bertankaynaroglu@hotmail.com, kaynaroglu@itu.edu.tr

B.Sc.: Aerospace Engineering at Istanbul Technical University

List of Publications and Patents:

- **B. Kaynaroğlu**, O. Tunçer, "Resolving Turbulent Flame Front from Mie Scattering Measurements", 09/2013, 8th Mediterranean Combustion Symposium, Çeşme, 08.09.2013 - 13.09.2013, Submitted to Journal of Thermal Science and Technology
- Tunçer, O., **Kaynaroğlu, B.**, Karakaya, M. C., Kahraman, S., Çetiner-Yıldırım, O., & Baytaş, C. (2014). Preliminary investigation of a swirl stabilized premixed combustor. *Fuel*, *115*, 870-874.
- Tuncer, O., **Kaynaroglu, B.** (2014). Experimental and numerical investigation of a swirl stabilized premixed methane/air flame. *Aircraft Engineering and Aerospace Technology*, *86*(3), 7-7.
- Kahraman S., **Kaynaroğlu B.**, O. Tunçer, "Investigation of Flow Passing Through A Swirl Wane by the Method of PIV Technique", 4. Ulusal Havacılık ve Uzay Konferansı(UHUK), İstanbul/Turkey, in Turkish.